IEEE Access
Multidisciplinary | Rapid Review | Open Access Journal

Received 24 January 2024, accepted 16 February 2024, date of publication 26 February 2024, date of current version 5 March 2024.

Digital Object Identifier 10.1109/ACCESS.2024.3370231

RESEARCH ARTICLE

Combining MIMO DBF With Automotive Synthetic Aperture Radar Imaging and Phase Error Correction

MASOUD FARHADI[1], (Graduate Student Member, IEEE), REINHARD FEGER[1], JOHANNES FINK[2], THOMAS WAGNER[1], (Member, IEEE), AND ANDREAS STELZER[1], (Member, IEEE)

[1]Institute for Communications Engineering and RF-Systems, Johannes Kepler University Linz (JKU Linz), 4040 Linz, Austria
[2]Corporate Sector Research and Advance Engineering, Robert Bosch GmbH, 70442 Stuttgart, Germany

Corresponding author: Masoud Farhadi (mas.farhadi@gmail.com)

ABSTRACT Automotive radar systems face challenges in generating high-resolution images that are essential for advancing autonomous driving technology. One promising solution to improve the angle resolution of radar images is the synthetic aperture radar (SAR) technique. However, achieving satisfactory SAR images involves overcoming difficulties such as high computational burden and accurate platform location determination. To address these challenges, we propose an innovative approach that integrates SAR imaging with digital beamforming (DBF) and multiple input multiple output (MIMO) techniques. The proposed approach significantly reduces the computational time required for SAR image formation and demonstrates superior phase error suppression compared to conventional methods. Our implemented algorithm reduces the number of radar samples and imaging complexity by up to a factor of 10 without compromising resolution and image quality. Furthermore, our proposed angle variant phase correction method can be used in challenging automotive scenarios to efficiently mitigate the effects of platform position inaccuracies and undesirable motions. Through simulations and practical experiments, we present promising results to highlight the advantages of combining real and synthetic apertures for radar imaging and phase error correction.

INDEX TERMS Automotive applications, beamforming, MIMO, phase error, radar imaging, synthetic aperture radar.

I. INTRODUCTION

Digital signal processing advancements have revolutionized radar systems by making them more powerful, compact, and cost-effective [1]. The upcoming generation of radar sensors is expected to produce high-resolution images for autonomous driving [2], [3], [4], [5]. However, the low angular resolution of reconstructed radar images remains a primary challenge in automotive applications [6], [7]. Therefore, researchers are working to improve the performance of radar sensors to enhance the perception of the surrounding area of a vehicle [8], [9].

The associate editor coordinating the review of this manuscript and approving it for publication was Shadi Alawneh.

To enhance the angular resolution and gather more information from an observed area, advanced radar systems utilize multiple channels to collect data from antenna arrays [5]. Data processing techniques such as multiple input multiple output (MIMO) and digital beamforming (DBF) offer undeniable advantages in various radar applications [10], [11], [12], [13], [14]. However, the angular resolution of radar images using a limited number of antennas may not be sufficient to meet the requirements of automotive applications. To address this issue, synthetic aperture radar (SAR) is a promising technique that can be used [15], [16].

SAR generates high-resolution radar images by moving a small radar system to create a large virtual aperture. This technique was initially developed for remote sensing

applications [17], [18], [19], but it has recently been proposed for various radar imaging purposes, including the automotive sector [20], [21], [22], [23]. However, adapting SAR image formation approaches for automotive applications is challenging due to the limited processing power and the maneuverability of a car [24], [25], [26], [27], [28].

To successfully reconstruct SAR images within a vehicle, it is essential to overcome two main challenges: high computational cost and inaccurate knowledge of platform positions. Current SAR approaches require more processing power than what is available in automobiles. Therefore, it is crucial to optimize and introduce new techniques in order to make SAR imaging feasible for automotive applications [29], [30], [31], [32]. Additionally, inevitable and unpredictable motions introduce phase errors that degrade image quality and target location accuracy. Estimating and correcting these phase errors is a demanding task but allows suppressing unwanted errors and improving image quality [33], [34], [35], [36], [37].

Researchers have been working on addressing the mentioned challenges and improving SAR imaging to make it more suitable for automotive applications. In recent years, several studies [31], [33], [38], [39], [40], [41], [42], [43], [44], [45] have reported progress in this area. However, there is still a missing piece in current research that we aim to address in our work. This involves utilizing the capabilities of available radar and positioning systems to reduce the complexity of image formation methods and simultaneously enhance image quality without major hardware or processing system modifications.

This work presents a novel method of integrating DBF and MIMO with SAR imaging to deliver high-resolution radar images. Our approach effectively reduces the computational burden of time-domain image formation compared to conventional methods such as backprojection (BP). Despite this reduction in computational effort, the image quality remains uncompromised by discarding redundant data and preserving all essential information. Moreover, the proposed image formation method is compatible with current automotive radar sensors. It uses existing hardware to perform DBF and MIMO processing efficiently and generate SAR images using data from all available antennas. Our approach reduces the slow-time radar samples and overall computational complexity of SAR imaging, making it suitable for in-car processing systems.

In this manuscript, we also discuss the challenge of estimating and correcting phase errors in radar images, which is essential for enhancing the quality of SAR images [16], [33], [35], [36], [46], [47]. Phase errors are caused by inaccurate platform locations and undesired movements, and they vary with the view angle, especially in automotive scenarios with a large field of view (FOV). Thus, it becomes crucial to focus on a specific region to mitigate these errors. To address this issue, our proposed method utilizes angular focusing to achieve efficient phase correction across the entire FOV. Therefore, this novel approach not only reduces computational cost but also suppresses the impact of positioning errors and car vibrations in the reconstructed images.

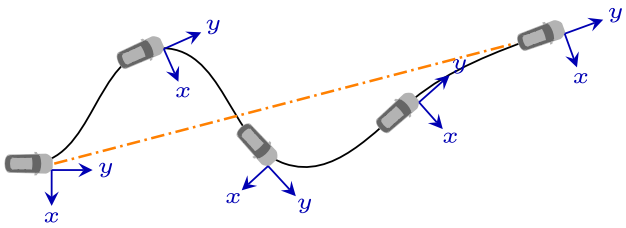

FIGURE 1. The black and orange lines represent the actual and ideal trajectories of a vehicle, respectively. To improve computational efficiency, frequency-based methods assume the ideal path, whereas time-domain image formation approaches use the actual positions. The *XY* coordinate system is displayed for each platform location.

We provide a concise overview of SAR image formation methods in Section II. Afterward, Section III describes the advantages of our novel approach by presenting fast radar imaging algorithms for automotive applications. Additionally, in Section IV, we explain phase error estimation techniques for automotive radar data and demonstrate how the proposed method enhances SAR image quality. Finally, the manuscript concludes by evaluating the use of multiple antennas for high-resolution radar imaging through simulations and measurements.

II. SAR IMAGE FORMATION

Different techniques have been suggested for reconstructing SAR images [17], [48], [49], which are categorized into two main groups: frequency-domain and time-domain. The most appropriate method is selected based on the particular application. In this section, we briefly analyze the advantages and disadvantages of these methods in the context of automotive SAR image formation.

Frequency-based methods are used to calculate images by making approximations, such as assuming equidistant sampling for the platform positions or a linear path for data acquisition, as shown in Fig. 1. These approximations make the algorithms computationally efficient, but they are not always suitable for all scenarios. For instance, in automotive SAR scenarios, data are usually collected from arbitrary and non-linear trajectories, and this makes obtaining high-quality SAR images a challenging task.

Frequency-based approaches can be used to generate SAR images by performing a 2D-fast Fourier transform (FFT) on the received signal, as explained in [50]. Although this method is computationally efficient, the quality of the image may be affected if assumptions such as constant velocity and straight trajectory are violated. To address this issue, time-domain approaches are used for automotive SAR imaging despite their higher computational complexity compared to frequency-domain algorithms [16], [41].

In the field of radar imaging, the BP algorithm is widely used for generating SAR images due to its ability to handle various data acquisition trajectories [38], [51]. In the

following section, we will introduce the equations and considerations involved in this imaging approach. This description will further be used in Section IV to provide a clear explanation of our method for estimating and correcting phase errors.

A. BACKPROJECTION

To reconstruct a SAR image using time-domain approaches, we need to integrate collected radar data from different platform positions coherently. Thus, by considering measured radar data from a single receiver as

$$x_{\mathrm{IF}}\left[n_{\mathrm{s}}, n_{\mathrm{f}}\right] = s_{\mathrm{IF}}\left[n_{\mathrm{s}}, n_{\mathrm{f}}\right] + \eta\left[n_{\mathrm{s}}, n_{\mathrm{f}}\right], \tag{1}$$

where n_{s} and n_{f} represent the slow-time and fast-time sample indices of radar data, and x_{IF} and s_{IF} are the measured and ideal signal model, respectively, and η indicates noise in the received radar data.

To generate SAR images, it is also necessary to determine the relative locations of the platform and of targets. As shown in Fig. 1, by considering a two-dimensional scenario in the XY plane, each point within the illuminated area is denoted in a Cartesian coordinate system as,

$$\mathbf{r}\left[p\right] = \begin{bmatrix} x\left[p\right] & y\left[p\right] & 0 \end{bmatrix}^{\mathrm{T}}, \tag{2}$$

where p represents the index of a pixel in an image and the transpose operator, denoted by $[.]^{\mathrm{T}}$, reverses the row and column indices of a matrix. It is important to note that the XY plane is defined with respect to the sensor coordinate system.

A vehicle can move along an arbitrary path to generate an automotive SAR image, as illustrated in Fig. 1. Therefore, it is essential to have a positioning system that can measure the platform's location. For this purpose, we use an Xsens MTi-G-710 sensor [52]. By combining data from global positioning system (GPS) and inertial measurement unit (IMU), we can estimate the position of the antenna phase center (APC) for each n_{s}, which can be denoted as

$$\mathbf{r}_{\mathrm{a}}\left[n_{\mathrm{s}}\right] = \begin{bmatrix} x_{\mathrm{a}}\left[n_{\mathrm{s}}\right] & y_{\mathrm{a}}\left[n_{\mathrm{s}}\right] & 0 \end{bmatrix}^{\mathrm{T}}, \tag{3}$$

where x_{a} and y_{a} indicate the antenna position in the Cartesian coordinate system.

As depicted in Fig. 2, the distance between the position of the radar sensor and each selected point in the observed area can be calculated as

$$d\left[n_{\mathrm{s}}, p\right] = \left\|\mathbf{r}_{\mathrm{a}}\left[n_{\mathrm{s}}\right] - \mathbf{r}\left[p\right]\right\|_2, \tag{4}$$

where $||\cdot||_2$ is the Euclidean-norm of a vector. By assuming that the radar platform does not move considerably during one chirp, the round-trip delay-time (RTDT) for the measured distance is given by,

$$\tau_{\mathrm{d}}\left[n_{\mathrm{s}}, p\right] = 2\frac{d\left[n_{\mathrm{s}}, p\right]}{c_0}, \tag{5}$$

where c_0 is the wave propagation speed.

Automotive radar systems typically utilize frequency-modulated continuous-wave (FMCW) signals to measure distances of objects [8], [23]. In this study, we utilize a 77 GHz radar system with a fast chirp modulation. The configurations of our radar system are summarized in Table. 1.

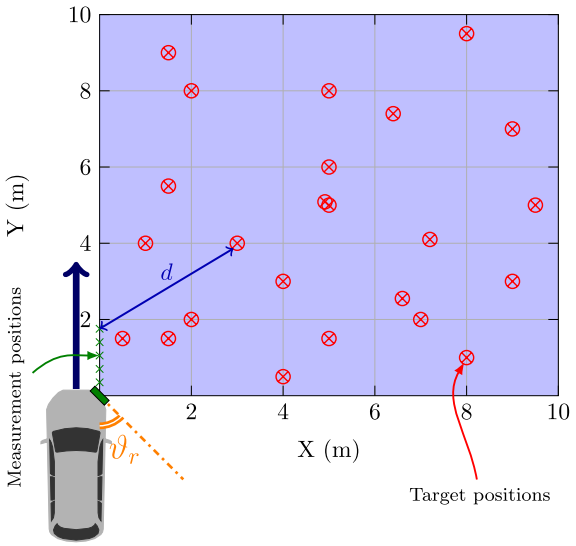

FIGURE 2. The sketch depicts a data acquisition structure with a radar system (green box) mounted on the car and simulated strong targets (red markers) in the observed area. The arrow in front of the car indicates the platform's motion direction, and ϑ_{r} represents the angle of the radar system relative to this direction, fixed at 45° in our scenarios.

TABLE 1. Parameters of the radar system.

RF carrier frequency	76.375 GHz
RF bandwidth	0.75 GHz
Single chirp duration	102.4 μs
Chirp repetition interval	112.4 μs
Fast time samples per chirp	512

To achieve coherent integration of fast-time and slow-time samples in SAR image formation approaches, we define two terms used to compress data in their respective domains. The range profile calculation is the initial step of an image reconstruction process. In our FMCW radar system, range profile data is computed through the Fourier transform of the received signal over the fast-time domain. To obtain the range profile data, x_{RP}, we utilize received radar signals, x_{IF}, as explained in [46]. Furthermore, time-domain image formation methods use the RTDT to align the received radar data from different platform locations. A corresponding term for each slow-time sample and the selected pixel of the image is defined as

$$\phi_{\mathrm{s}}\left[n_{\mathrm{s}}, p\right] = \exp\left(\mathrm{j}2\pi f_{\mathrm{c}}\tau_{\mathrm{d}}\left[n_{\mathrm{s}}, p\right]\right), \tag{6}$$

where f_{c} represents the center frequency of the chirp signal [49]. We use a radar sensor with N_{s} consecutive chirp signals in the slow-time domain and denote a vector for all slow-time samples as

$$\boldsymbol{\phi}_{\mathrm{s}}\left[p\right] = \left[\phi_{\mathrm{s}}\left[0, p\right], \cdots, \phi_{\mathrm{s}}\left[N_{\mathrm{s}} - 1, p\right]\right]^{\mathrm{T}}. \tag{7}$$

The range profile vector for an image pixel is defined as $\mathbf{x}_{\mathrm{RP}}[p]$, and is calculated based on samples of the range profile and RTDT defined by (5). A detailed explanation can be found in [46].

Finally, to generate a SAR image at the selected pixel location, the BP algorithm aligns range profile samples by the corresponding slow-time term as

$$I_{\mathrm{BP}}[p] = \boldsymbol{\phi}_{\mathrm{s}}^{\mathrm{H}}[p]\,\mathbf{x}_{\mathrm{RP}}[p]\,, \tag{8}$$

where $I_{\mathrm{BP}}[p]$ is a pixel of the SAR image which is calculated by compressing the slow-time data.

Calculating the value of each pixel in an image involves determining the RTDT of the selected point for every slow-time sample, and then aligning the corresponding range profile samples. This process creates a significant computational burden due to the nested loop that is required to iterate through all pixels and platform positions.

Researchers have proposed various solutions to mitigate the limitations of conventional time-domain image formation methods. For example, in [25], authors assume a constant velocity for the platform and similar distances for the radar positions for consecutive slow-time samples. This assumption simplifies the problem and allows for the use of a frequency-domain image reconstruction method. Furthermore, using an accurate positioning system in non-automotive scenarios can help to control radar locations and enhance the efficiency of imaging algorithms [20].

It is not practical to use the mentioned methods for automotive scenarios due to the required assumptions, such as constant velocity or equidistant sampling, which are not valid in all driving situations [24]. Furthermore, measuring accurate locations of a car requires highly precise sensors or restricting motions of the radar system. Therefore, nonlinear data collection paths in automotive scenarios lead to unacceptable phase errors and decreased image quality [21].

In our previous work [32], we introduced an approach to decrease the computational cost of automotive SAR imaging by reducing the required samples of the image formation procedure. As explained in the mentioned manuscript, this method requires recentering data before filtering and down-sampling, when applied to a short-range structure [32]. It is crucial to note that sample reduction should be based on eliminating redundant information without compromising image quality. In the following section, we provide a brief explanation of a sample reduction algorithm used to improve the efficiency of BP.

B. FAST BACKPROJECTION

The concept of fast BP algorithms is to reduce redundant information from radar data. These approaches aim to decrease the number of data samples and operations required to implement a fast version of the conventional algorithm [41], [53], [54]. A commonly used and efficient time-domain image formation method is fast factorized back-projection (FFBP), which adapts the BP approach to reduce the computational cost of SAR image formation [55].

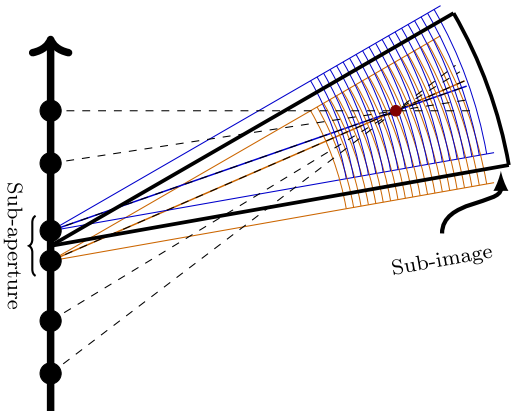

FIGURE 3. The FFBP reduces redundant radar data by grouping neighboring slow-time samples and creating beams for SAR image formation in multiple subimages. The algorithm is explained in [55].

The FFBP algorithm divides an observed area into small regions and calculates a SAR image in each of these subimages with a lower number of input samples. In [32], we presented a modified version of this approach to reconstruct an image with higher computational efficiency compared to the conventional method.

Fig. 3 shows that the sample reduction procedure of FFBP is similar to creating a beam using neighboring synthetic samples and replacing them with a decimated one. It divides the whole image into multiple subimages and reduces the number of collected samples in both slow-time and fast-time domains, based on the location of the selected region. Similarly, the platform locations are decreased, corresponding to the calculated samples. This technique is explained in detail in [55].

It is challenging to use FFBP for automotive radar imaging due to fundamental problems. Short-range geometry and wide FOV in automotive scenarios can cause a loss of essential information during the decimation procedure [32]. To address this issue, we need to implement a recentering algorithm as described in [32]. However, adapting the FFBP algorithm can retain necessary data only for low sample reduction factors.

To improve the efficiency of the SAR image formation algorithm for automotive applications, we suggest using a multi-channel radar system to create beams in different directions. This allows us to decrease the number of slow-time samples and improve SAR image quality by using DBF and a simple down-sampling method for radar data and platform positions. This feature will be explained in more detail in Section. III. Multichannel data increases system complexity, but it is already available in most automotive radars and can offer additional advantages, such as spatial filtering through MIMO and DBF [8], [11].

III. MULTI-CHANNELS AUTOMOTIVE SAR IMAGING

The primary objective of using multichannel radar data for SAR imaging is obtaining a high-quality radar image

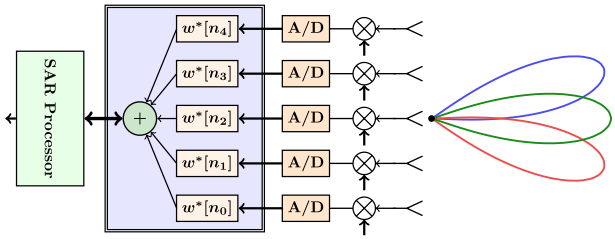

FIGURE 4. The schematic shows that the radar system employs multiple antennas and DBF to steer a beam. It can be seen that DBF uses different weights to generate beamformed data, which is then processed by the SAR block to reconstruct an image in the desired directions.

in a reasonable amount of time [39], [41]. To achieve this goal, one of the possible methods is utilizing the data from all antennas during the SAR imaging process by efficiently combining the real aperture data and then applying BP to the reduced data. This method allows for handling the significant computational costs that are associated with using all channels in conventional methods.

We propose implementing FFT-based DBF to merge real aperture data. Afterward, the synthetic aperture data and BP are used to generate a SAR image efficiently. The main advantages of our proposed method are combining synthetic and real aperture and using all of the available information in an efficient way for generating high-resolution radar images. In this section, we provide a detailed explanation of our approach by describing the combination of DBF with SAR image formation and validating this algorithm using simulation and experimental data. Furthermore, developing the idea of using a MIMO radar system in automotive SAR imaging is discussed at the end of this section.

Radar data for both our simulated and measured scenarios are collected using a platform that moves at a speed of 20 km/h along the Y-axis. Furthermore, all SAR images are calculated with 512×512 pixels and 1024 slow-time samples. The radar system has a chirp time of 112.4μs and we evaluate 1024 chirps for image formation. Thus, the coherent integration time for each image is 0.11 s and the aperture length is 0.64 m. In this manuscript, SAR images are normalized and illustrated with 50 dB dynamic range, in cases without color bar. Markers are used to indicate the actual locations of the simulated targets.

A. COMBINING DBF WITH SAR IMAGE FORMATION

DBF is widely used in automotive radar and SAR imaging [4], [7], [16], [39]. Due to the requirement of wide-angle imaging in automotive radar technology, the current trend in this field is toward using array processing and DBF [5], [56]. In this section, we briefly explain the concept of DBF and analyze the advantages of using a real antenna array for automotive SAR image formation.

Fig. 4 shows how an array of antenna elements can be used to create a beam towards a specific direction [57]. The DBF block implements a spatial filter by summing the received data after passing through calculated weights.

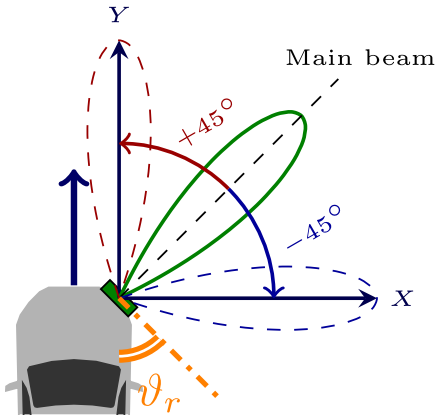

FIGURE 5. The radar system, which is mounted on the corner of the car, covers the observed area by changing the beam direction around the main beam. The angle of the main beam equals the rotation angle of the radar sensor, ϑ_r, with respect to the moving direction of the vehicle.

Our radar system uses beamforming to improve the computational efficiency of SAR imaging and suppress phase errors. To implement the concept of using DBF in automotive SAR imaging and reducing the computational complexity, we need to decrease the required samples of the image formation approach. To achieve this, we focus on a subregion of an image covered by a beam to use a small portion of the available data and reduce the overall processing burden.

The idea of subimage reconstruction using the DBF technique is inspired by the factorized image formation algorithms such as FFBP. In contrast to conventional factorized image reconstruction approaches, we select a subimage as an elliptical sector around the beam direction. Creating subimages by using the beam direction as the center angle of the sector and the beamwidth as the coverage area is a reasonable option. We use an FFT-based conventional beamforming (CBF) algorithm and down-sampling to reduce the computational cost of the image formation algorithm. Note that an additional filtering procedure before down-sampling, which would be required for the modified FFBP [32], is no longer necessary in the proposed approach.

The following simulations are done based on mechanically tilting the radar system 45° with respect to the driving direction. As shown in Fig. 5, this geometry allows us to digitally rotate the beam from -45 to $+45$ degrees to cover the intended area. We consider a small sector of an image to create a beam using CBF and focus on the targets in this region. Fig. 6 shows that beamforming helps us reconstruct the point-like targets in the selected beam direction while targets from other azimuth angles are suppressed. Slow-time sample reduction decreases the required time for image formation but it can cause ghost targets to appear outside of the interested region.

As shown in Fig. 6c, the DBF is applied to the received radar data. Since the main lobe is located towards the center of the illuminated area, only reflections of the targets in this region are retained in the SAR image. Using moderately down-sampled data can produce ambiguities and sidelobes

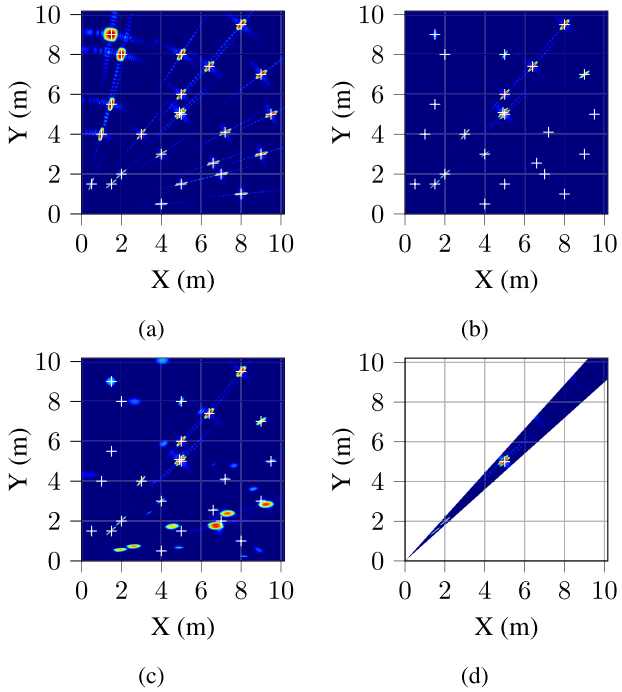

FIGURE 6. (a): Reconstructed BP image of the observed area. (b): Beamformed SAR image suppressed targets out of the desired direction. (c): Sample reduction (by factor four) creates blob-shaped sidelobes out of the main beam direction. (d): The desired targets are retained by sector image formation.

from targets. These sidelobes appear as blob-shaped distortions in areas outside the considered image sector. However, the image formation algorithm uses only the pixels within the selected area to generate a SAR image. Fig. 6d depicts that the sample reduction procedure does not cause any distortions within the reconstructed sector image. We use a combination of real and synthetic aperture, to achieve the required angle resolution. Combining beamformed data with synthetic antennas leads us to create high-resolution radar images that are suitable for use in automotive applications.

A radar image can be divided into multiple subimage sectors to cover the entire observed area. Our radar system has 16 receivers with half-wavelength spacing. Thus, we divide the illuminated region into 16 sectors and create a beam at each center angle. Each sector image is reconstructed using the BP algorithm, and all sectors are stitched together afterward. The center angle of a sector can be calculated as

$$\theta_c\left[n_{\text{sec}}\right] = \frac{\theta_{\text{FOV}}}{N_{\text{RX}}}\left(n_{\text{sec}} + \frac{1}{2}\right), \tag{9}$$

where θ_{FOV} is the angle of the defined FOV, N_{RX} denotes the number of receiver channels, and n_{sec} represents the index of the defined center angle that can be selected from $[0, \cdots, N_{\text{RX}} - 1]$.

The proposed idea aims to reduce the computational cost of radar imaging by taking advantage of a multi-receiver radar system. Using available capabilities in automotive SAR imaging allows us to keep the necessary slow-time samples

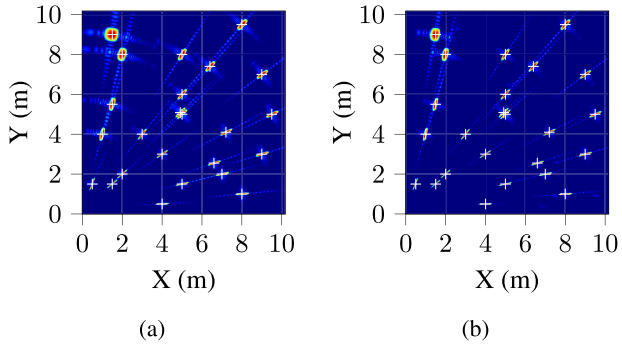

FIGURE 7. (a): The ideal SAR image from the simulated scenario is generated using BP. (b): The DBF-BP technique patches reconstruct subimage sectors together to decrease the processing time without sacrificing image quality.

and decrease the processing time. Moreover, our approach works for any structure of data collection without any modification because the nature of radar beams coincides with the shape of subimages. Other approaches, such as FFBP, need to calculate a decimation factor for each sub-image and modify radar data for the short-range target geometry.

The most significant point of the proposed approach, which we call DBF-BP, is using a computationally efficient implementation of DBF to reduce the processing burden of the conventional BP image formation algorithm. Fig. 7 shows that the quality of the DBF-BP image is even better than the conventional BP image. In addition, our algorithm does not impose any constraints on data collection or filtering processes for down-sampling.

There are two options for comparing our proposed approach with the conventional BP imaging. The first option is generating a BP image using all receivers and then comparing the image quality and the processing complexity. The second option is using only one receiver for BP image formation and evaluating both mentioned criteria. Using all receivers and the conventional BP method, as in the first option, would be unfair due to the strongly differing computational effort. Therefore, we have chosen the second option as it results in a similar computational burden.

It should be noted that the core concept of this approach is using all antenna channel information along with simple down-sampling to improve radar image quality without increasing the load on the main processing system. We utilize beamforming to coherently integrate the data from all receivers. This leads to a reduction of sidelobes in generated SAR image (Fig. 7b) compared to the conventional BP image (Fig. 7a). Using all receivers (in DBF-BP), provides significant benefits in terms of increasing signal to noise ratio (SNR) in comparison to a single receiver (in BP) with the same complexity.

Since the radar array structure is fixed, the processing burden of the proposed approach can be even reduced only by calculating FFT-based DBF in an efficient way on the available hardware of the sensor, which originally might be

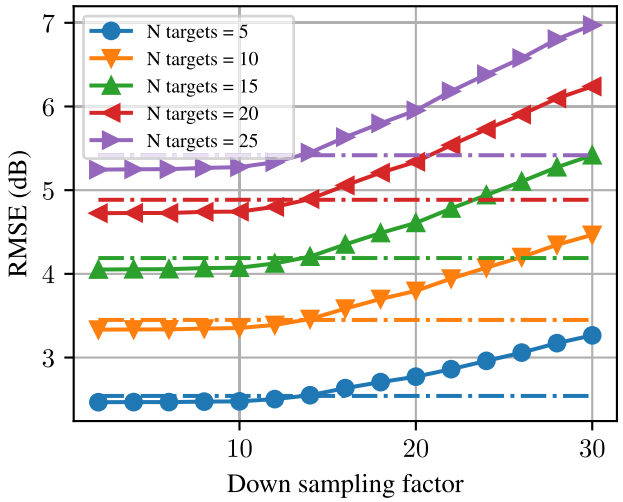

FIGURE 8. The RMSE of SAR images are computed by comparing them with ideal images using the same target locations. The value in the plot represents the mean value of RMSE of all iterations for each number of targets with random locations. The reference values, which are shown with dashed lines, are generated using BP. It can be seen that the DBF-BP algorithm with a downsampling factor up to 10 shows better image quality than BP.

designed for other applications. Therefore, the beamformed output data can be used for typical applications of a radar sensor and SAR image formation procedure simultaneously. As a result, we have a multi-functional radar sensor that is capable of generating high-resolution radar images from the illuminated area.

B. SIMULATION EVALUATIONS

To evaluate our proposed approach for general scenarios, we simulate several scenes using different numbers of targets placed at random uniform distributed locations. Moreover, ideal images with the same target positions are calculated. In these images, each reflector is modeled as a narrow Gaussian pulse in two dimensions. To determine the quality of reconstructed images in a quantitative manner, we compare them with the corresponding ideal images and compute an image quality metric, such as root mean square error (RMSE). To represent the image quality, we calculate a mean value of RMSE for each number of targets across all iterations. It can be seen in Fig. 8 that for all simulated scenarios, our approach with a downsampling factor up to 10 shows similar or even better image quality than the conventional BP. Overall, DBF-BP can generate SAR images of comparable quality to BP, but with a reduced computational time.

C. COMPUTATIONAL COMPLEXITY ANALYSIS

Quantitative evaluation of computational complexity could be done in two ways: Counting required operations, or running algorithms on the same hardware and comparing the run time. In this section, we present the required processing time and comparison of the computational effort of different algorithms.

TABLE 2. Computational time of different algorithms.

Downsampling factor	BP	FFBP	DBF-BP
1	29.7 s ±133 ms	30.8 s ±296 ms	28.9 s ±109 ms
2	-	24.6 s ±135 ms	14.6 s ±24 ms
4	-	17.1 s ±108 ms	7.4 s ±20 ms

The processing system uses an Intel core-i7-10700 CPU.

To evaluate the advantages of using DBF, we compare the processing time of our proposed algorithm with BP and FFBP. For a fair comparison, we intentionally implement all approaches without parallel or multiprocessing. Table. 2 shows the processing time of the DBF-BP method compared to the conventional BP and FFBP algorithms. It is important to point out that the FFBP method uses sample reduction in both slow-time and fast-time domains while the DBF-BP approach employs downsampling only in slow-time.

To quantitatively analyze the computational effort of the different algorithms, we also investigate their complexity based on the number of required operations. As an example, in [58] and [59], there are helpful comparisons between BP and FFBP. We also use a similar way for quantitative analysis of our proposed algorithm with other mentioned methods.

The basic operations of BP for each platform position and each image pixel location can be summarized as,

1) Range calculation from the sensor to the pixel location (subtraction and norm of a vector with three elements)
2) Interpolation of the calculated range to find the range index
3) Phase calculation based on the calculated range (multiplication of two complex values)
4) Applying phase compensation on the selected range profile value (a complex multiplication).

Instead of comparing the actual number of operations required by each approach, we propose comparing different algorithms proportionally, as the basic BP is the core element for all methods in our manuscript. Therefore, relative numbers of the imaging operations of the algorithms can be represented as,

- OP(Conventional BP) $\propto M \times N \times L$
- OP(FFBP) $\propto M \times N \times n_d \log_{n_d} L$ (if all sub-images can be decimated by n_d)
- OP(DBF-BP) $\propto M \times N \times L/n_d$

where $M \times N$ is the number of pixels of the reconstructed image (512×512), L is the number of platform positions (1024), and n_d is the sample reduction (decimation or downsampling) factor.

The critical point in our analysis is that we cannot accurately estimate the computational cost of FFBP for short-range scenarios. Due to the variation of the decimation factors for different subimages (between 1 and n_d), the complexity of FFBP can vary between the mentioned number of operations for BP (the worst case) and ideal FFBP (the best case).

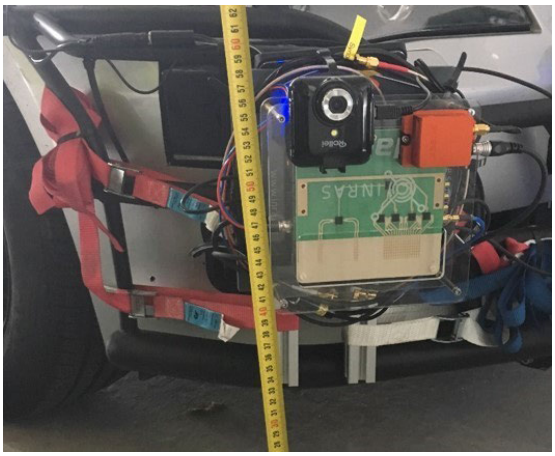

FIGURE 9. The radar and positioning system which are mounted on the front bumper of a car. In addition, a camera is added to the system to observe the measured area.

The issue of the FFBP for automotive applications and the required modifications (e.g., recentering data before filtering) are explained in detail in [32].

It is important to note that the additional minor operations, such as calculating the optimum values of n_{d} and filtering data in FFBP, are ignored in our calculation. This is because the image reconstruction operations are much more expensive than the neglected ones and take the major time of SAR image generation. In a similar way, the number of operations required for DBF can be neglected compared to the computational cost of SAR imaging. Since DBF can be implemented using a 1D FFT across all receiver channels for each platform location, the total number of operations is $(L/n_{\mathrm{d}}) \times N_{\mathrm{RX}} \log N_{\mathrm{RX}}$, where N_{RX} is the number of receiver channels. For instance, the required operations for our radar system, which includes 16 receivers, are $(L/n_{\mathrm{d}}) \times 64$. Therefore, the computational effort for DBF is much lower than the complexity of the rest of the SAR image formation.

DBF-BP image formation can exploit data of all channels and generate a SAR image with computational complexity similar to using one receiver and BP. In addition, we can reduce processing time and the number of slow-time samples through moderate down-sampling. The mentioned processing times of different approaches in Table 2 are matched to the quantitative analysis. The results indicate that the computational cost of our proposed approach is much lower than the other methods.

D. EXPERIMENTAL EVALUATIONS

We define a practical measurement scenario to evaluate our proposed method with experimental radar data. For this test, an FMCW radar system is mounted on the bumper of a car, as shown in Fig. 9. In the experiment, the relative locations of the platform are estimated using a position and navigation system. In the test area, we placed several metal poles at different distances to represent point-like targets in a SAR image. Fig. 10 shows a photo of an observed area and

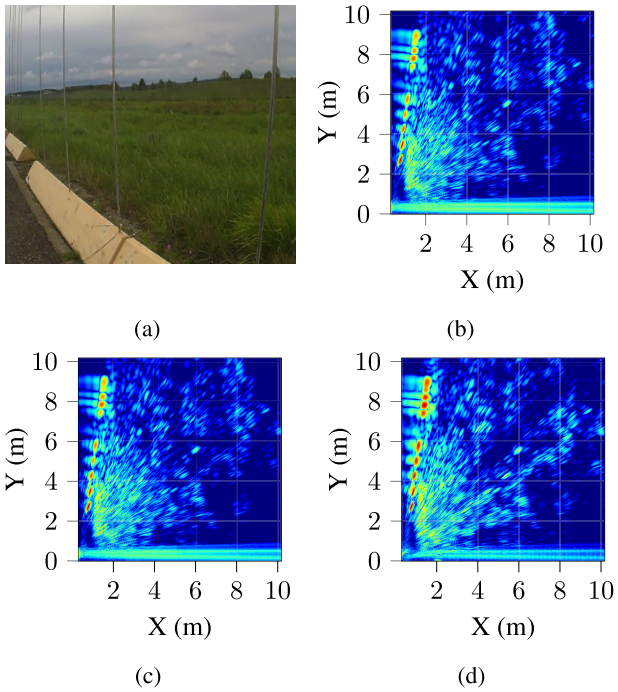

FIGURE 10. (a): A photo of the observed area shows the metal poles which are placed at the side of the road. (b): A SAR image, which is reconstructed using BP, indicate the poles as point-like targets. (c): An FFBP image is generated using sample reduction in both slow-time and fast-time domains by a factor of two. (d): The DBF-BP method creates a SAR image from the experimental data with the same downsampling factor and lower computational cost compared to conventional methods.

the reconstructed SAR image using the BP algorithm. The first position of the radar platform is the image origin, and the measurement configuration is similar to the simulation parameters.

As shown in Fig. 10a, the point-like targets in real scenarios are generated using metal poles in the observed area. In our simulation, we generated different numbers of point targets with random locations to analyze the proposed approach in a quantitative way. However, the number of targets is not restricted in the observed area and our algorithm works properly on real traffic scenarios because there is no special technique in our imaging procedure that depends on the number of targets.

Furthermore, we generate SAR images using the FFBP and our proposed method to compare the image quality and the processing time in a practical situation. Fig. 10 indicates that the quality of the images is not degraded by both methods, whereas the computational burden of the DBF-BP approach is much lower than FFBP.

Using a multichannel radar system and the DBF-BP algorithm for image formation reduces the complexity of the time-domain image formation. By creating different image sectors along the generated beams with the real aperture, we can decrease the number of synthetic aperture data without reducing SAR image quality. Moreover, this method helps us suppress phase errors more efficiently, as will be explained in Section IV.

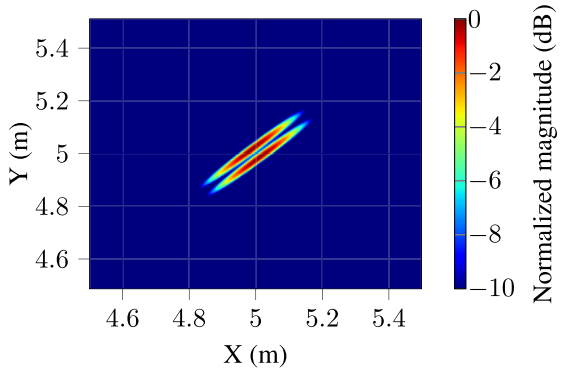

FIGURE 11. Reconstructed SAR image shows a scenario using two targets with 0.2° azimuth angle difference between them. It verifies the quantitative analysis of angular cross-range resolution.

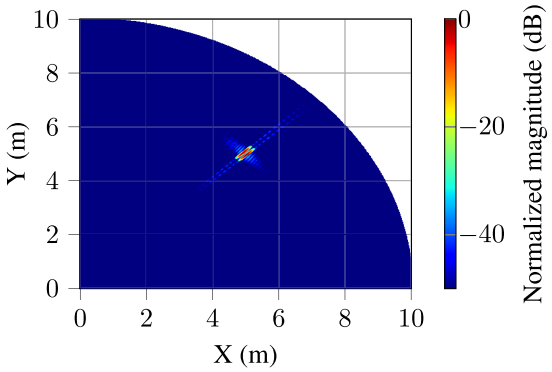

FIGURE 12. The reconstructed SAR image shows two targets at the center of the observed area with 1° azimuth angle difference between them.

E. ANGULAR RESOLUTION ANALYSIS

In processing of a SAR image, the distance which is perpendicular to the radar platform direction is influenced by the SAR processing approach. The resolution in this direction is called cross-range resolution because it is orthogonal to the range direction. The angular cross-range resolution (based on the positions of the nulls) can be written as,

$$\Delta\theta \approx \frac{\lambda}{2l_{\text{eff}}}, \tag{10}$$

where λ is the wavelength of the transmitted radar signal and l_{eff} is the length of the aperture where the echo signal from a scatterer can be received. It is called effective length and influences the cross-range resolution of the reconstructed SAR image. By considering the mentioned configuration of our simulation scenarios, where λ is 3.92 mm and l_{eff} equals 0.64 m, the achievable angular cross-range resolution for two targets is around 0.2°. We can verify the quantitative analysis by placing two targets at 0.2° difference in the observed area and reconstructing a SAR image, as shown in Fig. 11.

To suppress the sidelobes of targets and represent the reconstructed SAR image in a higher dynamic range, we apply a Taylor window in the slow-time domain. However, the azimuth broadening factor of the applied window causes a wider mainlobe and reduces the best achievable angular resolution. Therefore, for better visualization and compatibility with all simulated scenes, we generate a scenario by considering two targets with 1° difference in the observed area. We use this scenario to demonstrate the advantages of our proposed approach compared to the conventional SAR imaging methods. Furthermore, using a polar coordinate system for the image plane (pixel locations) and cutting the image at the range where targets are located help us to represent the results in one dimension and show the outstanding merit of the proposed method. Please note that the images are transferred to Cartesian coordinates for visualization. The SAR image of the explained scenario can be seen in Fig. 12.

To reduce the computational effort of the imaging process, one approach is to decrease the number of slow-time samples. This can be done by skipping the slow-time samples and subsampling the radar signal and platform positions. To compare our proposed approach with a BP imaging result, we generate images using the down-sampled data (e.g., by a factor of 8) from the defined scenario, as shown in Fig. 13. Selecting the image data at the defined range allows us to create a line plot for angle resolution evaluation, as shown in Fig. 14. The plot shows that down-sampling of slow-time radar data causes unwanted sidelobes in the selected range of the BP image (at the azimuth angle around 20°). However, the proposed approach can suppress them by using beamformed data for reconstructing each sub-image. It should be noted that our method can improve the image quality without sacrificing the resolution of the SAR image in the cross-range direction.

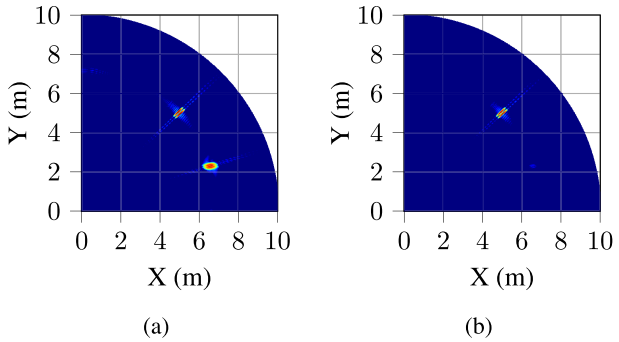

FIGURE 13. Two targets are located at the center of the simulated observed area with 1° azimuth angle difference. (a): A BP image by using down-sampled data (by a factor of 8) generates sidelobes in another location of the image. (b): Using DBF-BP with the same data keeps the targets and suppresses the sidelobes.

F. COMBINING MIMO WITH AUTOMOTIVE SAR IMAGING

MIMO is a technique that is widely used in automotive and robotic radar applications [4], [5], [8]. This technology improves the angular resolution and reduces the required aperture size of the radar sensor [10], [11], [12].

Comparing single-input multiple-output (SIMO) and MIMO radars for SAR image formation shows some superior aspects for MIMO systems, such as higher angular

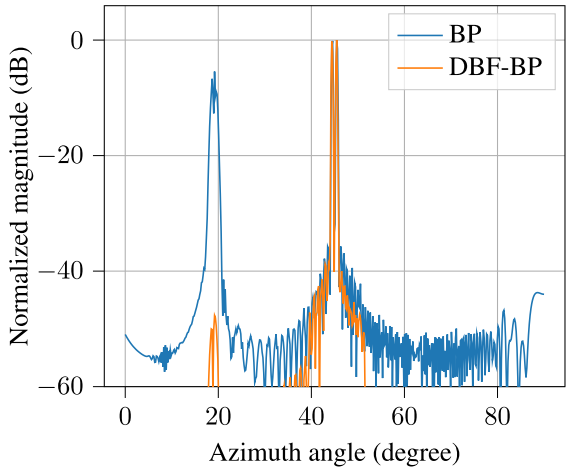

FIGURE 14. Cutting SAR images of BP and DBF-BP at the selected range shows that both approaches are able to distinguish two targets with 1° azimuth angle difference. However, BP causes sidelobes close to the target positions due to sample reduction, whereas the DBF-BP technique effectively suppresses them.

resolution [18], [42], [57]. However, hardware and processing complexity for a multi-transmitter system is higher than for a single transmitter [39], [60].

Due to the simplicity and practicability of time-division multiplexing (TDM) for FMCW signals, it is a widely used option for colocated automotive MIMO radars [61]. However, the main drawback of TDM-MIMO systems is the maximum unambiguous velocity of targets, which is also a critical factor in automotive SAR systems. In our recent work [62], we discussed the challenges of using TDM-MIMO radar systems and proposed our solution for MIMO-SAR image formation procedure.

Using time-domain image formation and complex summation of data from different receivers allows us to merge data from various locations. We can coherently integrate SAR images from different receivers to generate a MIMO backprojection (MIMO-BP) image, as explained in [62].

In our application, MIMO offers similar benefits to DBF in reducing the computational cost of the BP algorithm. However, the main advantage of a MIMO radar is its ability to provide high angular resolution with a small aperture size. Combining data of real and synthetic apertures helps to reduce the slow-time samples in the MIMO-SAR image formation procedure. This concept is similar to generating a DBF-BP image, but the size of the system is more suitable for automotive applications.

It is possible to improve the efficiency of the image formation procedure in MIMO-BP by using fewer slow-time samples. To reduce the computational burden of automotive SAR imaging, beamforming and downsampling can be applied to data of all virtual channels of a MIMO system. In Sections III-B and III-C, the quality and processing time of the multichannel imaging have been compared to the conventional approaches.

IV. PHASE ERROR ESTIMATION

This section analyzes automotive phase errors and their effects on SAR images. We focus on the group of methods that reduce phase errors only based on radar echo signals, called closed-loop approaches or particularly autofocusing.

A. AUTOFOCUS ALGORITHMS

Data-driven error estimation is a group of efficient approaches typically used in addition to motion compensation methods to improve the SAR image quality. These algorithms exploit radar data and refocusing techniques to suppress the effects of positioning inaccuracy.

In [63], different approaches are explained and compared to assess their functionality for various scenarios. On the one hand, methods, such as map drift (MD) [64], phase difference algorithm (PD) [64] and shift and correlation (SAC) [65], are simple and fit for secondary phase error but would need to be extended for higher order phase errors. On the other hand, non-model-based algorithms, such as phase gradient autofocus (PGA) [66], are robust and can estimate high-order phase errors. The authors conclude that the performance of an algorithm depends on the characteristics of phase errors and image scenes.

A suitable algorithm can be found based on the processing burden of the method and data collection scenarios. The most prominent approach for our application is PGA, which shows an exceptional capability to suppress various phase errors [47], [67]. The main inherent drawback of this method is assuming that the reconstructed image and the range profile can be converted to each other using a Fourier transform [36]. The strong scatterers in a SAR image are the essential points for phase error estimation. After generating the primary image, it is necessary to locate strong targets and align them. The standard PGA algorithm consists of four essential steps: circular shifting, windowing, phase kernel estimation, and iterative correction, which are explained in [46].

A novel method for phase error estimation is the generalized version of PGA, which overcomes difficulties of the standard method and shows satisfactory results for different experiments [68]. This algorithm originates from PGA and keeps the essential stages of the standard method with modifications, which are explained in [37].

B. SPACE-VARIANT PHASE ERRORS

Automotive SAR images typically cover a broad FOV with several short-range targets. It is not valid to assume that the same phase error applies to all pixels because phase errors differ across regions of a SAR image. In a practical automotive data collection, phase errors depend on the look angle and change along both the range and cross-range domains, and therefore, they are called space-variant, as shown in Fig. 15. One of the ideas to handle space-variant phase errors is applying the estimation procedure separately in different regions. Taking only a small region of the reconstructed image into account allows us to consider invariant phase error in the

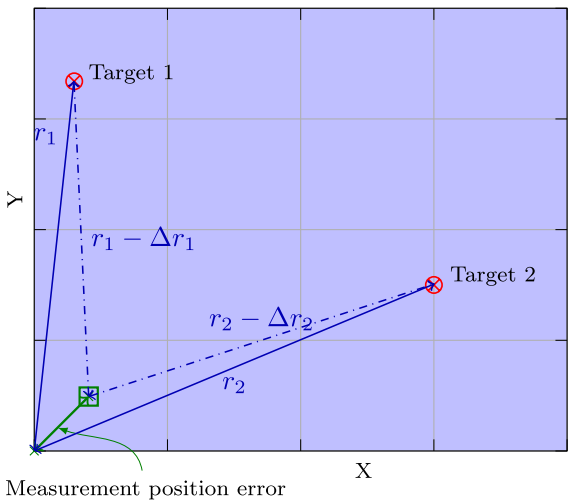

FIGURE 15. An example sketch of a practical automotive radar data collection shows two targets at the same range ($r_1 = r_2$) but in different regions. Phase errors for these targets are not the same and are changed based on the look angles.

selected area. Therefore, each sub-image includes data of targets with a similar error behavior [37].

V. AUTOMOTIVE PHASE ERROR CORRECTION

One of the essential procedures in high-quality automotive SAR imaging is phase error estimation and correction. However, correcting phase errors is challenging due to various reasons:

1) Wide FOV cause space-variant phase errors for different view angles.
2) The error suppression algorithm should be able to handle various positioning errors and car vibrations.
3) The computational complexity of the algorithm should be suitable for an affordable automotive processing system.

As previously stated, we utilize the BP image formation method for automotive SAR applications. Modifying this approach helps us to evaluate our idea of the space-variant phase error estimation. In this section, we elaborate on this concept by generating SAR images using various reconstruction approaches.

A. PHASE ERROR ESTIMATION ALGORITHM

In this section, we explain how generalized phase gradient autofocus (GPGA) technique generalizes the conventional PGA algorithm and modifies it to estimate and correct phase errors [68], as shown in Fig. 16.

The phase estimation kernel requires the information of strong point targets. Thus, we extract each selected point data from the input range profile as $\mathbf{x}_{\mathrm{RP}}\left[\tilde{p}\right]$, where $\tilde{p}$ indicates pixel indices of local maxima. GPGA multiplies the range profile data of the selected strong targets by the calculated slow-time term of these points, $\boldsymbol{\phi}_{\mathrm{s}}\left[\tilde{p}\right]$ as

$$\acute{\mathbf{x}}_{\mathrm{RP}}\left[\tilde{p}\right] = \boldsymbol{\phi}_{\mathrm{s}}^{*}\left[\tilde{p}\right] \odot \mathbf{x}_{\mathrm{RP}}\left[\tilde{p}\right], \tag{11}$$

where $\acute{\mathbf{x}}_{\mathrm{RP}}$ is the aligned range profile data and $\odot$ indicates element-wise multiplication.

The generalized method uses filtering operations to keep data of strong targets and rejects clutter. The filtered range profile is computed by applying a low pass filter (LPF) or multiplying a LPF matrix, $\mathbf{H}_{\mathrm{LPF}}$, on the compensated data as explained in [68],

$$\tilde{\mathbf{x}}_{\mathrm{RP}}\left[\tilde{p}\right] = \mathbf{H}_{\mathrm{LPF}}\acute{\mathbf{x}}_{\mathrm{RP}}\left[\tilde{p}\right], \tag{12}$$

where $\tilde{\mathbf{x}}_{\mathrm{RP}}$ contains the information of strong scatterers and suppresses noisy data from weaker targets.

Similar to the PGA approach, the normalized phase error gradient is estimated by the aligned and filtered range profile data as

$$\Delta\widehat{\phi}_{\mathrm{e}}\left[n_{\mathrm{s}}\right] = \angle\left(\sum_{\tilde{\mathrm{p}}} \tilde{x}_{\mathrm{RP}}\left[n_{\mathrm{s}}, \tilde{p}\right]\tilde{x}_{\mathrm{RP}}^{*}\left[n_{\mathrm{s}}-1, \tilde{p}\right]\right). \tag{13}$$

The integration of the estimated errors is calculated to find the phase error for each slow-time sample as

$$\widehat{\phi}_{\mathrm{e}}\left[n_{\mathrm{s}}\right] = \sum_{n=1}^{n_{\mathrm{s}}} \Delta\widehat{\phi}_{\mathrm{e}}\left[n\right]. \tag{14}$$

The last step of each iteration is applying the estimated phase error to the input range profile vector of the corresponding slow-time sample as

$$\hat{\mathbf{x}}_{\mathrm{RP}}\left[n_{\mathrm{s}}\right] = \mathbf{x}_{\mathrm{RP}}\left[n_{\mathrm{s}}\right]\exp\left(-\mathrm{j}\widehat{\phi}_{\mathrm{e}}\left[n_{\mathrm{s}}\right]\right), \tag{15}$$

where $\hat{\mathbf{x}}_{\mathrm{RP}}$ denotes the corrected range profile vector for all samples in the range domain.

B. PHASE ERROR CORRECTION

In this section, we discuss the integration of the phase error estimation approach and image formation methods, which are presented in Section III. In the first step of the evaluation process, we utilize a combination of BP and GPGA to estimate a simulated error that varies for different locations. To simulate a practical experiment, we introduce position errors to the platform locations instead of applying phase errors to the radar data. These position errors result in space-variant phase errors in the collected data.

We simulate sinusoidal position errors in both X and Y directions and add them to the platform positions. The sinusoidal frequency is 0.03 Hz, and the amplitude is around 0.8 mm. Fig. 17 shows the radar positions with and without error. The simulated position errors distort the reconstructed SAR image and generate high sidelobes around strong targets, as shown in Fig. 18a. Applying GPGA to the BP image suppresses phase errors and efficiently eliminates them in the center area of the image, while strong sidelobes have remained around target points in other regions, as shown in Fig. 18b. The primary drawback of this technique is its

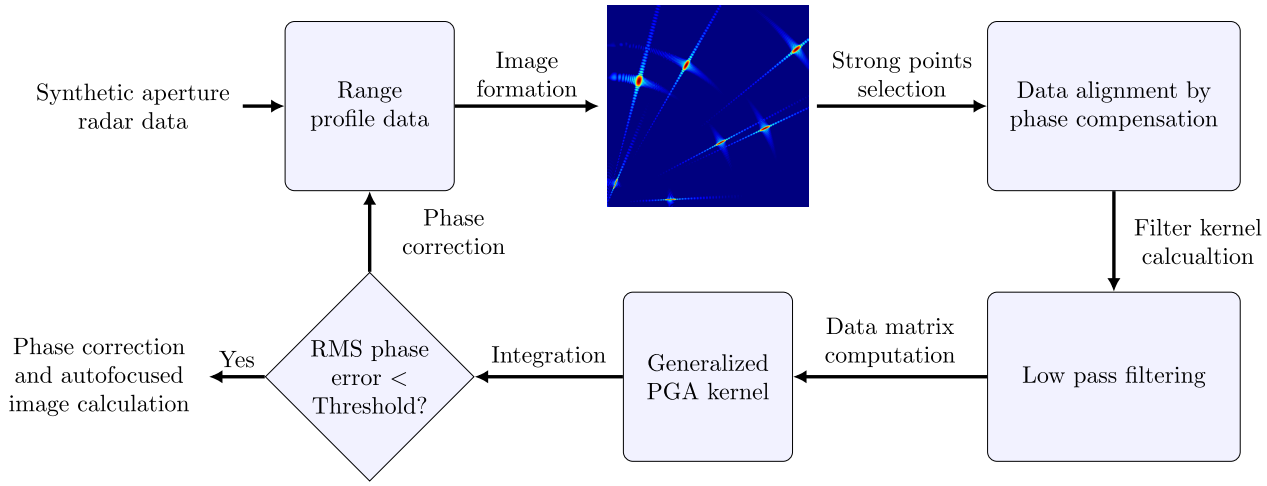

FIGURE 16. The block diagram of the GPGA approach preserves the four essential stages of the standard PGA, but modifies the blocks used for phase error estimation and correction.

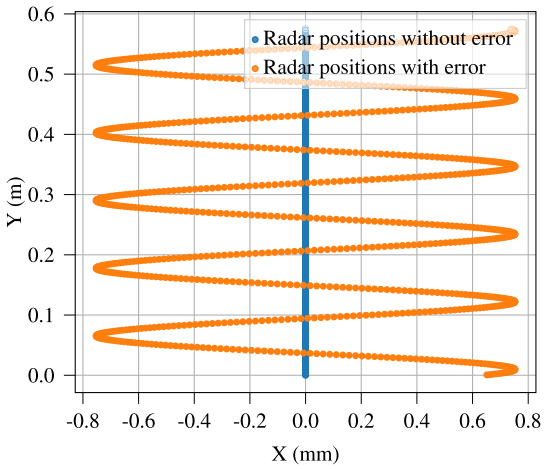

FIGURE 17. The radar locations with and without errors are shown in this plot. We generate the position errors by simulating two sinusoidal errors and adding them to the ideal platform positions in both dimensions.

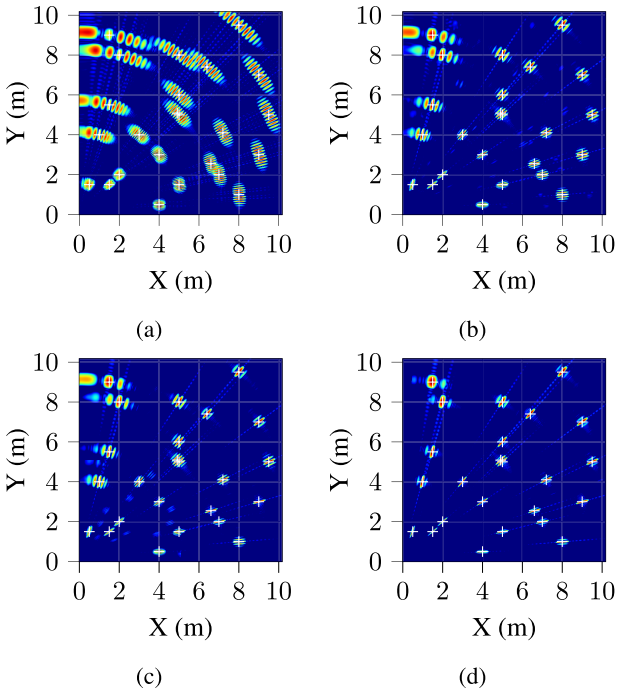

FIGURE 18. (a): A simulated BP SAR image shows the effect of space-variant phase errors on the reconstructed targets. (b): Applying the GPGA method to the BP image mainly corrects phase errors in the center region. (c): Combination of GPGA and FFBP suppresses the space-variant phase errors, but some errors are remaining. (d): A DBF-BP image shows space-variant phase error are effectively corrected using GPGA for beam-shaped image sectors.

reliance on estimating a single phase error for the entire image area. However, phase errors tend to behave differently in different regions, making it necessary to develop a method for correcting these variations.

We apply the GPGA algorithm to eliminate the space-variant phase errors that vary across different regions of a SAR image. The strong targets of each region can be used to estimate phase errors. Since a similar error influences the targets of one region, the correction procedure can efficiently suppress it. Fig. 18 depicts phase correction results using the FFBP and DBF-BP methods. The GPGA approach estimates and corrects phase errors on several sub-images independently. Since in our proposed image formation method, targets in a beam direction show a similar error behavior, the phase error correction algorithm leads to superior results compared to FFBP.

Furthermore, to evaluate the proposed algorithm for general cases, we simulate scenarios with different numbers of targets and various random locations. Fig. 19 shows that the MSE values of SAR images for the different random realizations of the simulated scene are reduced, leading to an improvement in image quality. It is worth noting that the reconstructed BP image with accurate platform locations is used as the reference image.

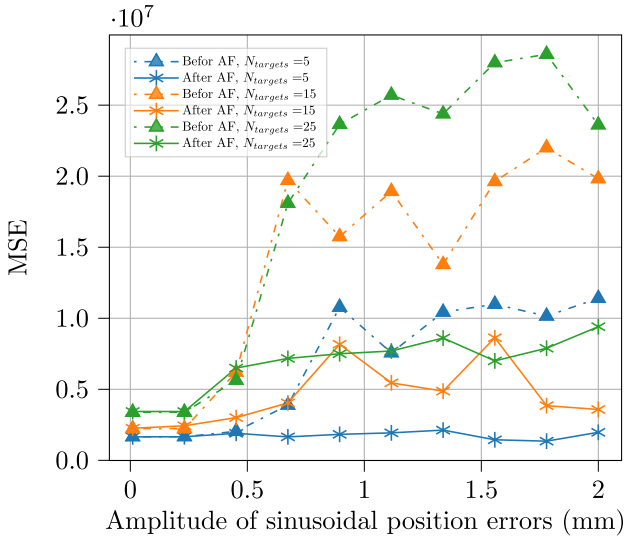

FIGURE 19. The mean square error (MSE) of reconstructed SAR images using the DBF-BP algorithm before and after autofocusing (AF). The ground truth image is generated using the accurate platform locations and BP. It can be seen that using our proposed method can reduce the MSE values and, therefore, improve the image quality for different numbers of targets with random locations.

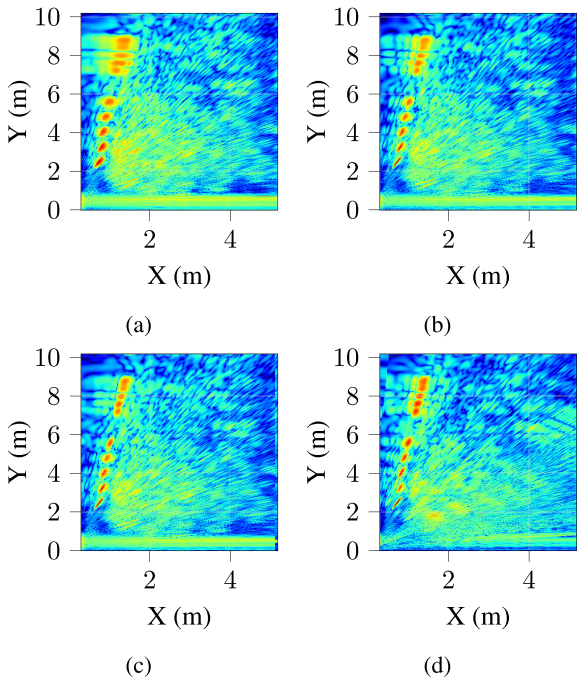

FIGURE 20. (a): A BP image is generated from radar measurement data without phase error correction. (b): A combination of GPGA and BP methods shows that targets are focused using phase error correction. (c): The GPGA method is applied on a FFBP image to focus on point-like targets. (d): Combination of GPGA and DBF-BP leads to the best result from the experimental data.

C. EXPERIMENTAL PHASE ERROR CORRECTION

To evaluate the proposed approach in a practical automotive radar data collection scenario, we mounted a 77 GHz radar system on a car, as shown in Fig. 9. In addition, Fig. 10a shows a series of metal poles that are installed in the observed area to generate point-like targets. An experiment with ten metal poles in the observed area is used to analyze the proposed combination of the image formation approaches and the phase estimation procedure. There are some primary steps to combine different localization sensors and filter the data to correct the position errors as much as possible.

The reconstructed images using the BP method and the phase error correction using GPGA are shown in Fig. 20b. In addition, a combination of GPGA and rectangular sub-images is used to correct phase errors in the measurement data. Fig. 20 indicates that the FFBP and DBF-BP method, generate focused images with the space-variant phase error estimation approach. Both methods are superior to the unsegmented phase compensated image, but using multichannel data and DBF-BP (or MIMO-BP) algorithm shows better phase error suppression compared to FFBP.

Our proposed image formation algorithms estimate phase errors more accurately than other approaches because of the use of beamformed data and beam-shaped sub-images that are compatible with the nature of the radar echo. It is worth noting that the approach is suitable for estimating and correcting the typical vibrations of a radar system in a car. However, solving the problem of complete dislocation of the radar antennas is beyond the scope of our investigation in this manuscript.

VI. CONCLUSION

In this paper, we have explored the idea of improving radar image quality and reducing computational burden by combining real and synthetic radar apertures. Our main objective was to evaluate the potential of utilizing multichannel radar systems with DBF and MIMO techniques for automotive SAR imaging. Employing a SIMO or a MIMO system allowed us to generate beamformed data and reduce the computational complexity of image formation by decreasing the amount of the required radar data by up to a factor of 10.

We also highlighted the significance of using multichannel radar systems for estimating different phase errors in various beam directions. Our research focused on developing a novel phase error correction algorithm to support multichannel data. We demonstrated that this approach could extract the phase error of the selected azimuth angle and efficiently correct space-variant phase errors for automotive SAR applications.

To assess our proposed approach, we simulated a scene including several targets with random locations. Positional errors were introduced to the platform locations in both range and cross-range dimensions. Additionally, we created a practical scenario for collecting automotive radar data with point-like targets. To conduct this experiment, a 77 GHz radar system was installed on a car and a series of metal poles were placed within the illuminated area. Our proposed technique proved to be more efficient compared to conventional algorithms in terms of computational burden and error correction.

In summary, we elaborated on utilizing DBF and MIMO techniques to create a SAR image in multiple directions by exploiting beamformed data. Our main contribution, presented in this work, was enhancing the quality of radar images while reducing the processing time. This was achieved by decreasing the computational complexity of SAR image formation and improving phase error suppression.

REFERENCES

[1] M. A. Richards, *Fundamentals of Radar Signal Processing*. New York, NY, USA: McGraw-Hill, 2014.

[2] J. Van Brummelen, M. O'Brien, D. Gruyer, and H. Najjaran, "Autonomous vehicle perception: The technology of today and tomorrow," *Transp. Res. C, Emerg. Technol.*, vol. 89, pp. 384–406, Apr. 2018.

[3] I. Bilik, O. Longman, S. Villeval, and J. Tabrikian, "The rise of radar for autonomous vehicles: Signal processing solutions and future research directions," *IEEE Signal Process. Mag.*, vol. 36, no. 5, pp. 20–31, Sep. 2019.

[4] J. Hasch, "Driving towards 2020: Automotive radar technology trends," in *IEEE MTT-S Int. Microw. Symp. Dig.*, Apr. 2020, pp. 1–4.

[5] S. M. Patole, M. Torlak, D. Wang, and M. Ali, "Automotive radars: A review of signal processing techniques," *IEEE Signal Process. Mag.*, vol. 34, no. 2, pp. 22–35, Mar. 2017.

[6] F. Engels, P. Heidenreich, A. M. Zoubir, F. K. Jondral, and M. Wintermantel, "Advances in automotive radar: A framework on computationally efficient high-resolution frequency estimation," *IEEE Signal Process. Mag.*, vol. 34, no. 2, pp. 36–46, Mar. 2017.

[7] T. Zhou, M. Yang, K. Jiang, H. Wong, and D. Yang, "MMW radar-based technologies in autonomous driving: A review," *Sensors*, vol. 20, no. 24, p. 7283, Dec. 2020.

[8] C. Waldschmidt, J. Hasch, and W. Menzel, "Automotive radar—From first efforts to future systems," *IEEE J. Microw.*, vol. 1, no. 1, pp. 135–148, Jan. 2021.

[9] F. Engels, P. Heidenreich, M. Wintermantel, L. Stäcker, M. Al Kadi, and A. M. Zoubir, "Automotive radar signal processing: Research directions and practical challenges," *IEEE J. Sel. Topics Signal Process.*, vol. 15, no. 4, pp. 865–878, Jun. 2021.

[10] J. Benesty, I. Cohen, and J. Chen, *Fundamentals of Signal Enhancement and Array Signal Processing*. Singapore: Wiley, Dec. 2017.

[11] S. Sun, A. P. Petropulu, and H. V. Poor, "MIMO radar for advanced driver-assistance systems and autonomous driving: Advantages and challenges," *IEEE Signal Process. Mag.*, vol. 37, no. 4, pp. 98–117, Jul. 2020.

[12] G. Hakobyan and B. Yang, "High-performance automotive radar: A review of signal processing algorithms and modulation schemes," *IEEE Signal Process. Mag.*, vol. 36, no. 5, pp. 32–44, Sep. 2019.

[13] F. Harrer, F. Pfeiffer, A. Löffler, T. Gisder, C. Buchberger, and E. Biebl, "Multi channel approaches for an automotive synthetic aperture radar," in *Proc. 11th German Microw. Conf. (GeMiC)*, Mar. 2018, pp. 391–394.

[14] J. Benesty, *Array Processing: Kronecker Product Beamforming*. Berlin, Germany: Springer, 2019.

[15] T. S. S. Nag, G. S. Vandana, B. Pardhasaradhi, and P. Srihari, "SAR imaging with automotive radar: Range migration algorithm, experiment, and future directions in automotive vehicle," in *Proc. IEEE 7th Int. Conf. Recent Adv. Innov. Eng.*, vol. 7, Dec. 2022, pp. 382–387.

[16] S. Tebaldini, M. Manzoni, D. Tagliaferri, M. Rizzi, A. V. Monti-Guarnieri, C. M. Prati, U. Spagnolini, M. Nicoli, I. Russo, and C. Mazzucco, "Sensing the urban environment by automotive SAR imaging: Potentials and challenges," *Remote Sens.*, vol. 14, no. 15, p. 3602, Jul. 2022.

[17] A. Moreira, P. Prats-Iraola, M. Younis, G. Krieger, I. Hajnsek, and K. P. Papathanassiou, "A tutorial on synthetic aperture radar," *IEEE Geosci. Remote Sens. Mag.*, vol. 1, no. 1, pp. 6–43, Mar. 2013.

[18] G. Krieger, S. Huber, M. Villano, F. Q. D. Almeida, M. Younis, P. Lopez-Dekker, P. Prats, M. Rodriguez-Cassola, and A. Moreira, "SIMO and MIMO system architectures and modes for high-resolution ultra-wide-swath SAR imaging," in *Proc. 11th Eur. Conf. Synth. Aperture Radar*, Jun. 2016, pp. 1–6.

[19] M. Younis, C. Fischer, and W. Wiesbeck, "Digital beamforming in SAR systems," *IEEE Trans. Geosci. Remote Sens.*, vol. 41, no. 7, pp. 1735–1739, Jul. 2003.

[20] M. E. Yanik, D. Wang, and M. Torlak, "Development and demonstration of MIMO-SAR mmWave imaging testbeds," *IEEE Access*, vol. 8, pp. 126019–126038, 2020.

[21] J. W. Smith and M. Torlak, "Efficient 3-D near-field MIMO-SAR imaging for irregular scanning geometries," *IEEE Access*, vol. 10, pp. 10283–10294, 2022.

[22] A. Sengupta, F. Jin, R. A. Cuevas, and S. Cao, "A review of recent advancements including machine learning on synthetic aperture radar using millimeter-wave radar," in *Proc. IEEE Radar Conf.*, Sep. 2020, pp. 1–6.

[23] J.-W. Ting, D. Oloumi, and K. Rambabu, "FMCW SAR system for near-distance imaging applications—Practical considerations and calibrations," *IEEE Trans. Microw. Theory Techn.*, vol. 66, no. 1, pp. 450–461, Jan. 2018.

[24] D. Tagliaferri, M. Rizzi, M. Nicoli, S. Tebaldini, I. Russo, A. V. Monti-Guarnieri, C. M. Prati, and U. Spagnolini, "Navigation-aided automotive SAR for high-resolution imaging of driving environments," *IEEE Access*, vol. 9, pp. 35599–35615, 2021.

[25] R. Feger, A. Haderer, and A. Stelzer, "Experimental verification of a 77-GHz synthetic aperture radar system for automotive applications," in *Proc. ICMIM*, Mar. 2017, pp. 111–114.

[26] C. Wang, J. Pei, M. Li, Y. Zhang, Y. Huang, and J. Yang, "Parking information perception based on automotive millimeter wave SAR," in *Proc. IEEE Radar Conf.*, Apr. 2019, pp. 1–6.

[27] T. Gisder, M.-M. Meinecke, and E. Biebl, "Synthetic aperture radar towards automotive applications," in *Proc. 20th Int. Radar Symp. (IRS)*, Jun. 2019, pp. 1–10.

[28] M. Farhadi, R. Feger, J. Fink, T. Wagner, and A. Stelzer, "Synthetic aperture radar imaging of moving targets for automotive applications," in *Proc. 18th European Radar Conf.*, Apr. 2022, pp. 453–456.

[29] T. Kan, G. Xin, L. Xiaowei, and L. Zhongshan, "Implementation of real-time automotive SAR imaging," in *Proc. IEEE 11th Sensor Array Multichannel Signal Process. Workshop (SAM)*, Jun. 2020, pp. 1–4.

[30] H. Iqbal, A. Löffler, M. N. Mejdoub, D. Zimmermann, and F. Gruson, "Imaging radar for automated driving functions," *Int. J. Microw. Wireless Technol.*, vol. 13, no. 7, pp. 682–690, Apr. 2021.

[31] M. Hoffmann, T. Noegel, C. Schüßler, L. Schwenger, P. Gulden, D. Fey, and M. Vossiek, "Implementation of real-time automotive SAR imaging," 2023, *arXiv:2306.09784*.

[32] M. Farhadi, R. Feger, J. Fink, M. Gonser, J. Hasch, and A. Stelzer, "Adaption of fast factorized back-projection to automotive SAR applications," in *Proc. Eur. Radar Conf.*, Oct. 2019, pp. 261–264.

[33] M. Manzoni, D. Tagliaferri, M. Rizzi, S. Tebaldini, A. V. M. Guarnieri, C. M. Prati, M. Nicoli, I. Russo, S. Duque, C. Mazzucco, and U. Spagnolini, "Motion estimation and compensation in automotive MIMO SAR," *IEEE Trans. Intell. Transp. Syst.*, vol. 24, no. 2, pp. 1756–1772, Feb. 2023.

[34] Y. Bao, T. Mahler, A. Pieper, A. Schreiber, and M. Schulze, "Motion based online calibration for 4D imaging radar in autonomous driving applications," in *Proc. German Microw. Conf. (GeMiC)*, Mar. 2020, pp. 108–111.

[35] T. Gisder, M.-M. Meinecke, and E. Biebl, "Algorithmic steps for SAR backprojection on radar based motion estimation," in *Proc. 21st Int. Radar Symp. (IRS)*, Oct. 2020, pp. 385–390.

[36] A. Evers and J. A. Jackson, "A comparison of autofocus algorithms for backprojection synthetic aperture radar," in *Proc. IEEE Int. Radar Conf.*, Apr. 2020, pp. 821–826.

[37] M. Farhadi, R. Feger, J. Fink, T. Wagner, M. Gonser, J. Hasch, and A. Stelzer, "Space-variant phase error estimation and correction for automotive SAR," in *Proc. Eur. Radar Conf.*, Jan. 2021, pp. 310–313.

[38] S. Tebaldini, M. Rizzi, M. Manzoni, A. M. Guarnieri, C. Prati, D. Tagliaferri, M. Nicoli, U. Spagnolini, I. Russo, and C. Mazzucco, "SAR imaging in automotive scenarios," in *Proc. Microw. Medit. Symp. (MMS)*, May 2022, pp. 1–5.

[39] B. Zhang, G. Xu, R. Zhou, H. Zhang, and W. Hong, "Multi-channel back-projection algorithm for mmWave automotive MIMO SAR imaging with Doppler-division multiplexing," *IEEE J. Sel. Topics Signal Process.*, vol. 17, no. 2, pp. 445–457, Mar. 2023.

[40] M. G. Polisano, M. Manzoni, S. Tebaldini, A. Monti-Guarnieri, C. M. Prati, and I. Russo, "Very high resolution automotive SAR imaging from burst data," *Remote Sens.*, vol. 15, no. 3, p. 845, Feb. 2023.

[41] M. Manzoni, S. Tebaldini, A. V. Monti-Guarnieri, C. M. Prati, and I. Russo, "A comparison of processing schemes for automotive MIMO SAR imaging," *Remote Sens.*, vol. 14, no. 19, p. 4696, Sep. 2022.
[42] X. Gao, S. Roy, and G. Xing, "MIMO-SAR: A hierarchical high-resolution imaging algorithm for mmWave FMCW radar in autonomous driving," 2021, *arXiv:2101.09293*.
[43] S. Lee, Y. Jung, M. Lee, and W. Lee, "Compressive sensing-based SAR image reconstruction from sparse radar sensor data acquisition in automotive FMCW radar system," *Sensors*, vol. 21, no. 21, p. 7283, Nov. 2021.
[44] T. Grebner, R. Riekenbrauck, and C. Waldschmidt, "Simultaneous localization and mapping (SLAM) for synthetic aperture radar (SAR) processing in the field of autonomous driving," *IEEE Trans. Radar Syst.*, vol. 2, pp. 47–66, 2024.
[45] S.-W. Kang, H.-J. Cho, and S. Lee, "Deep learning-based motion compensation for automotive SAR imaging," *Measurement*, vol. 224, Jan. 2024, Art. no. 113862.
[46] M. Farhadi, R. Feger, J. Fink, T. Wagner, M. Gonser, J. Hasch, and A. Stelzer, "Phase error estimation for automotive SAR," in *IEEE MTT-S Int. Microw. Symp. Dig.*, Nov. 2020, pp. 1–4.
[47] C. V. Jakowatz, D. E. Wahl, P. H. Eichel, D. C. Ghiglia, and P. A. Thompson, *Spotlight-Mode Synthetic Aperture Radar: A Signal Processing Approach: A Signal Processing Approach*. Boston, MA, USA: Springer, 1996.
[48] A. Reigber, R. Scheiber, M. Jager, P. Prats-Iraola, I. Hajnsek, T. Jagdhuber, K. P. Papathanassiou, M. Nannini, E. Aguilera, S. Baumgartner, R. Horn, A. Nottensteiner, and A. Moreira, "Very-high-resolution airborne synthetic aperture radar imaging: Signal processing and applications," *Proc. IEEE*, vol. 101, no. 3, pp. 759–783, Mar. 2013.
[49] A. Meta, P. Hoogeboom, and L. P. Ligthart, "Signal processing for FMCW SAR," *IEEE Trans. Geosci. Remote Sens.*, vol. 45, no. 11, pp. 3519–3532, Nov. 2007.
[50] R. Feger, C. Wagner, S. Schuster, S. Scheiblhofer, H. Jager, and A. Stelzer, "A 77-GHz FMCW MIMO radar based on an SiGe single-chip transceiver," *IEEE Trans. Microw. Theory Techn.*, vol. 57, no. 5, pp. 1020–1035, May 2009.
[51] A. Ribalta, "Time-domain reconstruction algorithms for FMCW-SAR," *IEEE Geosci. Remote Sens. Lett.*, vol. 8, no. 3, pp. 396–400, May 2011.
[52] *Xsens MTi-710 GNSS/INS*. Accessed: May 4, 2023. [Online]. Available: https://www.movella.com/products/sensor-modules/xsens-mti-g-710-gnss-ins
[53] Q. Dong, G.-C. Sun, Z. Yang, L. Guo, and M. Xing, "Cartesian factorized backprojection algorithm for high-resolution spotlight SAR imaging," *IEEE Sensors J.*, vol. 18, no. 3, pp. 1160–1168, Feb. 2018.
[54] K. E. Dungan, L. A. Gorham, and L. J. Moore, "SAR digital spotlight implementation in MATLAB," *Proc. SPIE*, vol. 8746, May 2013, Art. no. 87460A.
[55] L. M. H. Ulander, H. Hellsten, and G. Stenstrom, "Synthetic-aperture radar processing using fast factorized back-projection," *IEEE Trans. Aerosp. Electron. Syst.*, vol. 39, no. 3, pp. 760–776, Jul. 2003.
[56] S. Wang, H. Chen, V. M. Patel, and A. Petropulu, "Two-dimensional beamforming automotive radar with orthogonal linear arrays," in *Proc. IEEE Radar Conf. (RadarConf)*, Boston, MA, USA, Apr. 2019, pp. 1–6.
[57] G. Krieger, M. Younis, S. Huber, F. Bordoni, A. Patyuchenko, J. Kim, P. Laskowski, M. Villano, T. Rommel, P. Lopez-Dekker, and A. Moreira, "Digital beamforming and MIMO SAR: Review and new concepts," in *Proc. 9th Eur. Conf. Synth. Aperture Radar*, Apr. 2012, pp. 11–14.
[58] L. M. Ulander, H. Hellsten, and G. Stenstroem, "Performance analysis of fast backprojection for synthetic-aperture radar processing," *Proc. SPIE*, vol. 4382, pp. 13–21, Aug. 2001.
[59] D. E. Wahl, D. A. Yocky, and C. V. Jakowatz Jr., "An implementation of a fast backprojection image formation algorithm for spotlight-mode SAR," *Proc. SPIE*, vol. 6970, Apr. 2008, Art. no. 69700H.
[60] G. Krieger, "MIMO-SAR: Opportunities and pitfalls," *IEEE Trans. Geosci. Remote Sens.*, vol. 52, no. 5, pp. 2628–2645, May 2014.
[61] S. Hamidi, M.-R. Nezhad-Ahmadi, and S. Safavi-Naeini, "TDM based virtual FMCW MIMO radar imaging at 79GHz," in *Proc. 18th Int. Symp. Antenna Technol. Appl. Electromagn. (ANTEM)*, Aug. 2018, pp. 1–2.
[62] M. Farhadi, R. Feger, J. Fink, T. Wagner, and A. Stelzer, "Automotive synthetic aperture radar imaging using TDM-MIMO," in *Proc. IEEE Radar Conf.*, May 2021, pp. 1–6.
[63] R. Yang, H. Li, S. Li, P. Zhang, L. Tan, X. Gao, and X. Kang, *Autofocus Algorithm for SAR*. Singapore: Springer, 2018, pp. 407–427.
[64] W. C. Carrara, W. G. Carrara, R. S. Goodman, and R. M. Majewski, *Spotlight Synthetic Aperture Radar: Signal Processing Algorithms*. Norwood, MA, USA: Artech House, 1995.
[65] J. Dall, "A fast autofocus algorithm for synthetic aperture radar processing," in *Proc. IEEE Int. Conf. Acoustics, Speech, Signal Process.*, vol. 3, Mar. 1992, pp. 5–8.
[66] D. E. Wahl, P. H. Eichel, D. C. Ghiglia, and C. V. Jakowatz, "Phase gradient autofocus—A robust tool for high resolution SAR phase correction," *IEEE Trans. Aerosp. Electron. Syst.*, vol. 30, no. 3, pp. 827–835, Jul. 1994.
[67] V. C. Koo, T. S. Lim, and H. T. Chuah, "A comparison of autofocus algorithms for SAR imagery," in *Proc. Prog. Electromagn. Res. Symp.*, 2005, p. 4.
[68] A. Evers and J. A. Jackson, "A generalized phase gradient autofocus algorithm," *IEEE Trans. Comput. Imag.*, vol. 5, no. 4, pp. 606–619, Dec. 2019.

MASOUD FARHADI (Graduate Student Member, IEEE) was born in Isfahan, Iran, in 1986. He received the B.S. and M.S. degrees in electronic engineering from the Amirkabir University of Technology (Tehran Polytechnic), Tehran, Iran, in 2009 and 2012, respectively. He is currently pursuing the Ph.D. degree in electronics and information technology with Johannes Kepler University Linz, Austria. In 2018, he joined the Institute for Communication Engineering and RF-Systems, Johannes Kepler University Linz, as a Research Assistant.

REINHARD FEGER was born in Kufstein, Austria, in 1980. He received the Dipl.-Ing. (M.Sc.) degree in mechatronics and the Dr.Techn. (Ph.D.) degree in mechatronics from Johannes Kepler University Linz, Linz, Austria, in 2005 and 2010, respectively.

In 2005, he joined the Institute for Communications and Information Engineering, Johannes Kepler University Linz, as a Research Assistant. In 2007, he became a member of the Christian Doppler Laboratory for Integrated Radar Sensors, Johannes Kepler University Linz. He is currently an Associate Professor with the Institute for Communications Engineering and RF-Systems, Johannes Kepler University Linz. His research interests include radar signal processing and radar system design for industrial and automotive radar sensors. He was a recipient of the 2011 Microwave Prize and the 2011 German Microwave Conference Best Paper Award. In 2012, he received the Best Measurement Paper Prize at the European Conference on Antennas and Propagation.

JOHANNES FINK was born in Geislingen, Germany, in 1984. He received the Dipl.Ing. (M.Sc.) and Dr.-Ing. (Ph.D.) degrees in electrical engineering and information technology from Karlsruhe Institute of Technology, Karlsruhe, in 2011 and 2017, respectively. From 2011 to 2017, he was with the Communication Engineering Laboratory, Karlsruhe Institute of Technology. Since 2017, he has been with the Corporate Sector Research and Advance Engineering, Robert Bosch GmbH, in the field of radar systems and signal processing. His research interests include radar system design for industrial and automotive radar systems and radar signal processing.

THOMAS WAGNER (Member, IEEE) was born in Linz, Austria, in 1985. He received the Dipl.Ing. (M.Sc.) degree in mechatronics from Johannes Kepler University Linz, Linz, in 2011. Since 2011, he has been with the Institute for Communications and Information Engineering, Johannes Kepler University Linz, as a Research Assistant, where he became a member of the Christian Doppler Laboratory for Integrated Radar Sensors.

ANDREAS STELZER (Member, IEEE) received the Diploma in Engineering degree in electrical engineering from the Technical University of Vienna, Vienna, Austria, in 1994, and the Dr.Techn. (Ph.D.) degree (Hons.) in mechatronics from Johannes Kepler University Linz, Austria, in 2000.

In 2003, he became an Associate Professor with the Institute for Communications Engineering and RF Systems, Johannes Kepler University Linz. In 2007, he was with the Christian Doppler Research Laboratory for Integrated Radar Sensors. Since 2008, he has been a Key Researcher with the Austrian Center of Competence in Mechatronics (ACCM), Linz, where he is responsible for numerous industrial projects. Since 2011, he has been a Full Professor with Johannes Kepler University Linz, where he is currently heading the Department of RF-Systems. He has authored or coauthored over 420 journal articles, conference papers, and workshop contributions. His research interests include microwave sensor systems for industrial and automotive applications, integrated radar sensor concepts, SiGe-based circuit design, microwave packaging in embedded wafer level ball grid array (eWLB), RF and microwave subsystems, surface acoustic wave (SAW) sensor systems and applications, and digital signal processing for sensor signal evaluation.

Dr. Stelzer is a member of the Austrian ÖVE. He is also a member of the IEEE Microwave Theory and Techniques (MTT) Society, the IEEE Instrumentation and Measurement (IM) Society, and the IEEE Circuits and Systems (CAS) Society. He was a recipient of several awards, including the 2008 IEEE MTT Society (IEEE MTT-S) Outstanding Young Engineer Award, the 2011 IEEE Microwave Prize, and the Best Paper Award of the *International Journal of Microwave and Wireless Technologies* (IJMWT), in 2016. He was a recipient of the 2012 European Conference on Antennas and Propagation (EuCAP) Best Measurement Paper Prize, the 2012 Asia–Pacific Conference on Antennas and Propagation (APCAP) Best Paper Award, the 2011 German Microwave Conference (GeMiC) Best Paper Award, the EEEfCOM Innovation Award, and the European Microwave Association (EuMA) Radar Prize of the European Radar Conference (EuRAD), in 2003. He was the Chair of the MTT-27 Wireless-Enabled Automotive and Vehicular Applications and the IEEE International Conference on Microwaves for Intelligent Mobility, in 2020. He has served as an Associate Editor for IEEE Microwave and Wireless Components Letters. He has served as an IEEE Distinguished Microwave Lecturer, from 2014 to 2016.